ANISOTROPY AND STRUCTURING OF ROUGH-WALL TURBULENT FLOWS

Takahiro Miura, Koji Matsubara, Atsushi Sakurai
Department of Mechanical and Production Engineering,
Niigata University
Ikarashi 2-no-cho 8050, Nishi-ku, Niigata-shi 950-2181, Japan
f09k008c@mail.cc.niigata-u.ac.jp

ABSTRACT

Direct numerical simulations were performed for turbulent flows in the spatial developing region of a ribbed channel, where square ribs were attached to one wall. The rib pitch-to-height ratio was changed at three steps; Pi/H = 2, 4 and 7. The bulk Reynolds number was given 4,560 through simulations. For the same parameters, simulations were also made for periodic fully developed cases. Although the friction factor decreased as flow goes downstream in the case of Pi/H = 2, it increased after unsteadiness in the case of Pi/H = 7 due to the turbulence enhancement. For Pi/H = 7, the developing flow near the rough wall even in the second cavity had a similar structure to the fully developed flow, whereas developed structures extended further away from the ribbed wall. The vortex structures were revealed by instantaneous fields and the two-point correlation of vorticities. Streamwise and spanwise vortices appeared near the rough wall. The streamwise vortex was smaller than that in a smooth channel, especially in the streamwise direction, and the inclination angle of the vortex was larger. Although the flow near the ribs was more isotropic than the smooth wall, coherent structures existed and produced the high correlation between the streamwise and wall-normal velocity fluctuations.

INTRODUCTION

The turbulent flow over a rough wall is important subject for engineers and researchers since this type of flows is encountered in many practical applications, e.g., the internal cooling of a gas-turbine blade and the electronics cooling. Therefore, fully developed turbulence in a roughened channel has been keenly examined in existing experiments and simulations.

Leonardi et al. (2004) directly solved the basic equations for the rough-wall turbulence, and pointed out that longitudinal structures near the smooth wall are deformed by the wall roughness to spread in the lateral direction. Recently, Ashrafian and Andersson (2006), Ikeda and Durbin (2007) performed DNS of similar situation. The latter group reported on turbulence statistics including intensity of vorticity fluctuation. However, the detail of coherent structures is still ambiguous, and characteristics in a spatially developing region are left unknown due to scarcity of the previous works. It is expected to reveal these unexplored matters since such efforts are thought to shed light on the turbulence modeling and the constructing methodology of turbulence control.

In the present study, numerical simulations are made for spatial advancement of rough channel turbulent flows. All the essential scale of turbulence is solved by fine grid meshes without turbulence models. Examination is given to how the flow features, turbulence statistics and structures grow under influence from the repeated ribs.

NOMENCLATURE

b_{ij} : Reynolds stress anisotropy tensor
C_f : skin friction coefficient
f : apparent friction factor
H : height of rib
k : turbulent kinetic energy
L_x, L_z : computational domain sizes in x and z directions
N_x, N_y, N_z : grid numbers in x, y and z directions
Pi : rib pitch
p : pressure
Q : second invariant of velocity-gradient tensor
Re_m : bulk Reynolds number, $2U_m\delta/\nu$
Re_{max} : Reynolds number, $U_{max}\delta/\nu$
Re_τ : friction Reynolds number, $U_\tau\delta/\nu$
t : time
U_m : bulk mean velocity
U_{max} : maximum velocity
U_τ : friction velocity, $(\tau_w/\rho)^{1/2}$
u_i : velocity in x_i direction
u, v, w : velocity in x, y and z directions
x_i : coordinate in the i th direction; x_1, x_2 and x_3 denote x, y and z
x, y, z : streamwise, wall-normal and spanwise coordinates
Δx, Δy, Δz : grid spacings in x, y and z directions
δ : channel half width
δ_{ij} : Kronecker delta
ν : kinematic viscosity
ρ : density
τ_w : wall shear stress
ω_i : vorticity in x_i direction

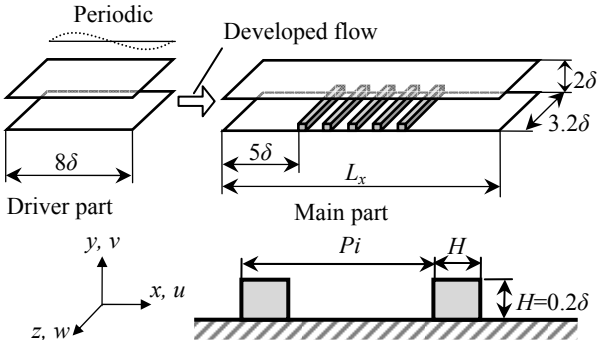

Figure 1. Computational domain and coordinate system for developing cases.

Table 1. Computational conditions for developing cases.

Case	1	2	3
Pi/H	2	4	7
Rib number	19	10	5
$Re_{\tau 0}$	150	150	150
L_x/δ	12.7	12.7	19.0
N_{x0}	64	64	64
N_x	768	768	768
$\Delta x_0/\delta$	0.125		
$\Delta x/\delta$	0.00625-0.0625		

Subscripts and Superscripts

- $(\,)_0$: value in driver part or inlet
- $(\,)_r$: value on rough-wall side
- $(\,)_{rms}$: root-mean-square value
- $(\,)_s$: value on smooth-wall side
- $(\,)'$: fluctuating component
- $\overline{(\,)}$: ensemble average over z direction and time
- $\langle(\,)\rangle$: average in x direction

NUMERICAL METHOD

We computed both developing and fully developed flows in ribbed channels.

Developing Flow

Figure 1 shows the computational domain and the coordinate system. The square ribs are placed on one wall of the channel with constant pitch for each computed case. The fully developed turbulent flow in the smooth channel is simulated in the driver part by assuming the streamwise periodicity, and this is provided to the inlet of the ribbed channel. No-slip condition is applied to all the solid walls, and the periodic boundary condition is used in the spanwise direction of the driver and the ribbed channel. The convection out-flow equation

$$\frac{\partial u_i}{\partial t} + U_c \frac{\partial u_i}{\partial x} = 0 \tag{1}$$

is solved at the exit of the ribbed channel, where U_c is the bulk mean velocity at the boundary.

The basic equations treated are the continuity and Navier-Stokes equations for the incompressible fluid:

$$\frac{\partial u_j}{\partial x_j} = 0\,, \tag{2}$$

$$\frac{\partial u_i}{\partial t} + u_j \frac{\partial u_i}{\partial x_j} = -\frac{1}{\rho}\frac{\partial p}{\partial x_i} + \nu \frac{\partial^2 u_i}{\partial x_j \partial x_j}\,. \tag{3}$$

The fractional step method (Kim and Moin, 1985) is used as the algorithm: the Crank-Nicolson scheme for the wall-normal second derivatives and the second order Adams-Bashforth scheme for other terms. Forth order finite difference is used for the approximation of the spatial derivatives (Matsubara et al., 1998). In the driver part, the Poisson's equation for the pressure is solved by the fast Fourier transformation (FFT) in the streamwise and spanwise directions and by the TDMA with the fourth-order compact finite difference in the wall-normal direction. In the main part, the Poisson's equation is computed by the FFT in the only spanwise direction and by the successive over-relaxation method in the other directions.

Table 1 shows the numerical condition and the grid resolution. The rib height, H, is kept constant at $H/\delta = 0.2$. The rib pitch, Pi, is changed at three steps; $Pi/H = 2$, 4 and 7. The rib number, N, for each case is selected so that the ribbed length, $(Pi/H)N$, exceeds 35. The friction Reynolds number at the inlet, $Re_{\tau 0}$, is assigned at 150. The corresponding bulk Reynolds number, Re_m, is approximately 4560. The grid data in the streamwise direction are as Table 1. The grids in the wall-normal and spanwise directions are the same in all the cases: $N_y = 98$, $N_z = 64$, $\Delta y/\delta = 0.00625$-$0.0667$ and $\Delta z/\delta = 0.05$. The computational grids are allocated finely near the walls and in the ribbed channel, especially dense in upstream of the front surface of the rib. Single-rib simulations using this kind of resolution agreed well with an experiment and with a fine-grid simulation, and the numerical code and the grids were validated (Miura et al., 2010a).

Fully Developed Flow

Fully developed flows are simulated in the same way as the developing cases, except that streamwise periodicity is assumed without the driver part. The computational conditions

are listed in Table 2. Three cases treat the same rib shapes as the developing flows, and one case is added for comparison with an experiment. The mean friction Reynolds number, Re_τ, is selected for $Re_m \approx 4560$ in each case. The computational grids are the same as downstream ribbed channel in the developing cases.

Profiles of the rough-wall mean velocity normalized by the rough-wall friction velocity are shown in Figure 2. The present result and the experimental data by Hanjalić and Launder (1972) have the same rib pitch, i.e., $Pi/H = 10$. The logarithmic function, have been used by Hanjalić and Launder,

$$\left\langle \overline{u}_r^+ \right\rangle = \frac{1}{0.42} ln\left(\frac{y}{H}\right) + 3.2 \,, \qquad (4)$$

is also shown in the figure. Although the Reynolds number of the present case is lower than a tenth of that for the experiment, the mean velocity profiles agree well above $y/H \approx 2$. Validity of the present DNS is confirmed.

RESULTS AND DISCUSSION

Friction Factor

In Figure 3, presentation is made for the apparent friction factor:

$$f = \frac{\int_0^{2\delta}\left(\overline{p} + \frac{\rho \overline{u}_i \overline{u}_i}{2}\right)\overline{u}dy\Big|_{x=x_u} - \int_0^{2\delta}\left(\overline{p} + \frac{\rho \overline{u}_i \overline{u}_i}{2}\right)\overline{u}dy\Big|_{x=x_d}}{\rho U_m{}^3 (x_d - x_u)} \,. \qquad (5)$$

As suggested by the equation, f essentially means the mechanical energy loss. In Figure 3, f is computed for each cavity, selecting reference positions x_u and x_d on the middle of upstream and downstream ribs of the cavity. The origin in the streamwise direction is located at the front surface of the first rib. The figure illustrates that the value of f decreases as flow goes downstream in the case of $Pi/H = 2$ and, however, it oscillates to show alternating rise and fall in $Pi/H = 7$. In the latter, f is considered to increase in further downstream since the fully developed value is larger than that of the developing area. In the case of $Pi/H = 4$, f is almost constant, and the trend of f is medium between other cases. The decreasing of f is observed also in laminar flows due to thickening of the boundary layer, and the trends in $Pi/H = 4$ are consistent with it. On the other hand, increasing of f in $Pi/H = 7$ contradicts the laminar theory, implying the complexity of turbulent flows.

Turbulent Kinetic Energy

Figure 4 shows contours of turbulent kinetic energy for $Pi/H = 2$ and $Pi/H = 7$. In the case of $Pi/H = 2$, the turbulent energy is large only near the first rib, and change of the boundary layer thickness is thought to dominate the pressure loss as earlier mentioned. In the case of $Pi/H = 7$, the turbulent energy gradually increases into the developed value, and the increased turbulence is thought to collect the fast fluid into the near wall layer enhancing the pressure loss.

Table 2. Computational conditions for fully developed cases.

Case	F-1	F-2	F-3	F-4
Pi/H	2	4	7	10
Rib number	16	8	5	4
Re_τ	185	240	300	300
L_x/δ	6.4	6.4	7.0	8
N_x	512	512	560	640
$\Delta x/\delta$	0.0125			

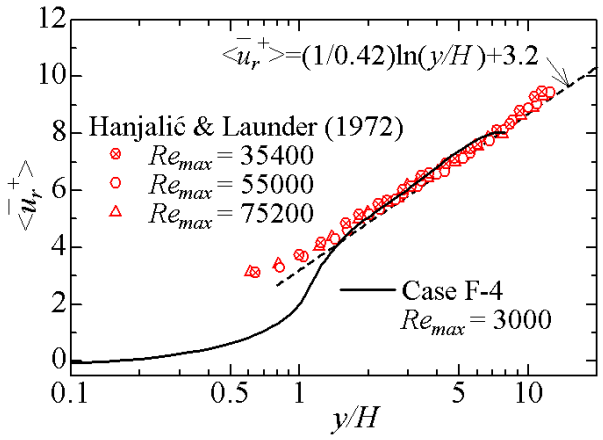

Figure 2. Rough-wall mean velocity profiles for fully developed flow.

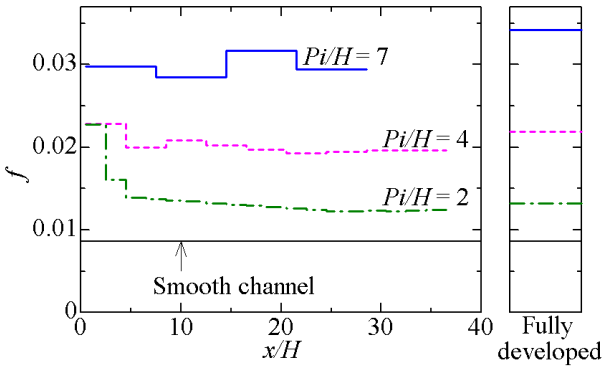

Figure 3. Apparent friction factor from mid-crest to next mid-crest.

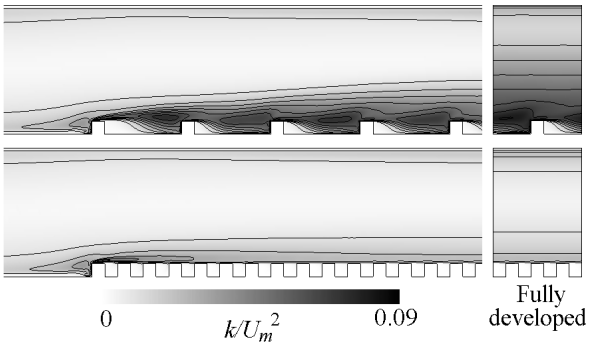

Figure 4. Contours of turbulent kinetic energy. One contour level denotes 0.01. Top: $Pi/H = 7$, bottom: $Pi/H = 2$.

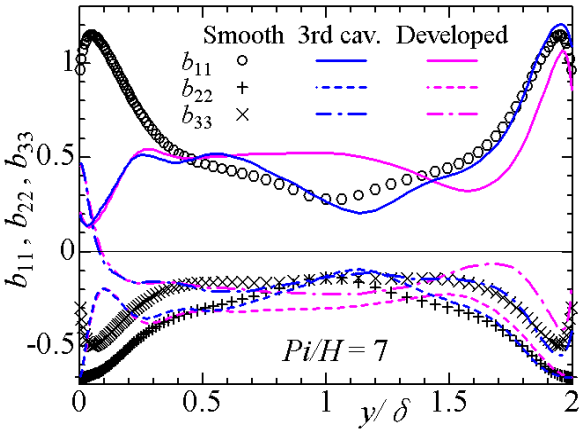

Figure 5. Reynolds normal stress anisotropy tensor at each mid-cavity.

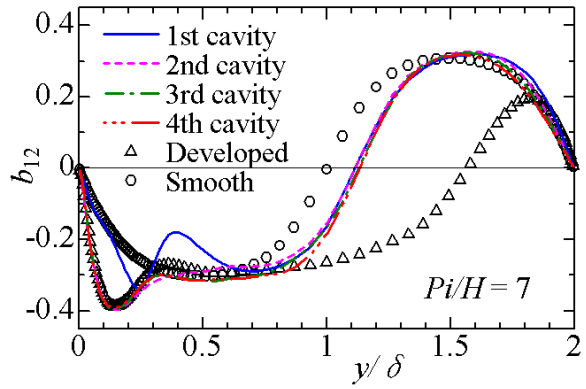

Figure 6. Reynolds shear stress anisotropy tensor at each mid-cavity.

Anisotropy

Previous investigations in fully developed flow of ribbed channel (Leonardi et al., 2004; Ashrafian and Andersson, 2006; Ikeda and Durbin, 2007) have reported that turbulence anisotropy near the rough wall is reduced as compared to the smooth wall. This has been shown by the Reynolds stress anisotropy tensor:

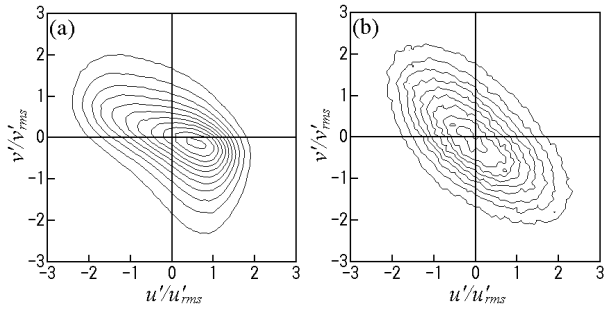

Figure 7. Joint probability distributions of u'/u'_{rms} and v'/v'_{rms}. (a) Smooth channel, $y/\delta \approx 0.13$; (b) Case F-3, near mid-cavity, $y/\delta \approx 0.2$.

$$b_{ij} = \frac{\overline{u_i' u_j'}}{k} - \frac{2}{3}\delta_{ij} \,. \qquad (6)$$

For isotropic turbulence, each b_{ij} should be zero. Profiles of the Reynolds normal stress anisotropy tensor at the middle of each cavity for $Pi/H = 7$ are shown in Figure 5. The anisotropy tensors near the rough wall in the developing flow are almost same as in the fully developed flow and are closer to zero with respect to the smooth wall. However, as suggested in Figure 6 of the Reynolds shear stress anisotropy tensor, b_{12}, the correlation between u' and v' increases near the rough wall. This enhancement of the Reynolds shear stress anisotropy is shown in also previous DNSs (Ashrafian and Andersson, 2006; Ikeda and Durbin, 2007).

To present details of the high correlation, the joint probability distributions of u' and v' normalized by each root-mean-square are shown in Figure 7. The selected positions of y are near maximum turbulent kinetic energy. Near the smooth wall, large negative u' correlate with positive v', and large negative v' correlate with positive u'. However, negative u' correlate with positive v' of similar magnitude near the rough wall.

Vortex Structure

To observe the vortex structures, iso-surfaces of the second invariant of the velocity-gradient tensor are presented in Figure 8. In the smooth channel, there are streamwise fine scale vortices as pointed out by the earlier workers (Jeong et al., 1997). In the developing flow of the rough channel, spanwise vortices are shed from the first rib, and the streamwise vortices gradually increase as the flow goes downstream. Even in the second cavity, the spanwise vortices and streamwise vortices appear densely, and the swift transition from spanwise to streamwise structures is suggested to occur. The fully developed flow of the ribbed channel has a similar structure to the developing flow; however, developed structures extend further away from the wall.

Figure 9 shows profiles of the Root-mean-square vorticity fluctuations at each mid-cavity. The vorticity fluctuations in developing flow resemble that of the fully developed flow below $y/\delta = 0.4$. The $\omega'_{z,rms}$ have a local maximum near the

rough wall like the $\omega'_{x,rms}$. This corresponds to the presence of the spanwise vortices.

Figure 10 shows the two-point conditional correlation of ω'_x:

$$R_{\omega_x\omega_x} = \frac{\overline{\omega'_x\left(x_{ref}, y_{ref}, z\right)\omega'_x\left(x, y, z + i\Delta z\right)}}{\omega'_{x,rms}\left(x_{ref}, y_{ref}\right)\omega'_{x,rms}\left(x, y\right)} \quad (7)$$

$$i = \begin{cases} 1 & for\ \omega'_x\left(x_{ref}, y_{ref}, z\right) \geq 0 \\ -1 & for\ \omega'_x\left(x_{ref}, y_{ref}, z\right) < 0 \end{cases}$$

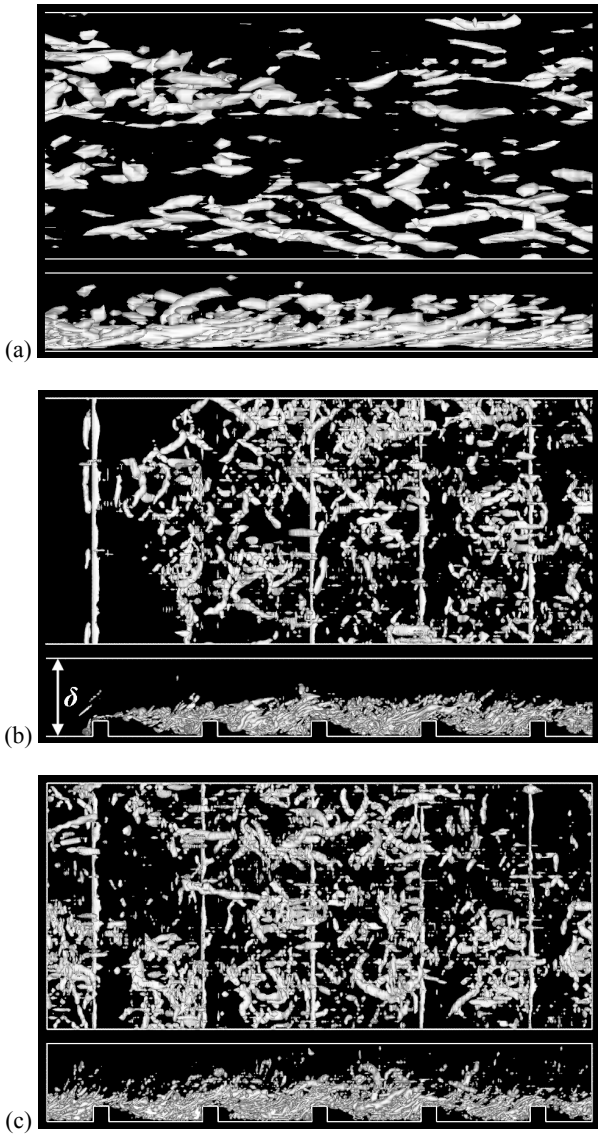

Figure 8. Vortex structure visualized by iso-surfaces of second invariant, Q. Flow is left to right. (a) Smooth channel, $Q\delta^2/U_m^2 = 1$; (b) Case 3, $Q\delta^2/U_m^2 = 40$; (c) Case F-3, $Q\delta^2/U_m^2 = 40$.

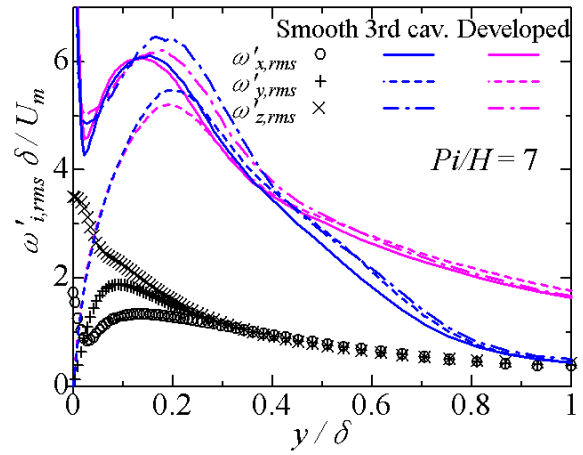

Figure 9. Root-mean-square vorticity fluctuations at each mid-cavity.

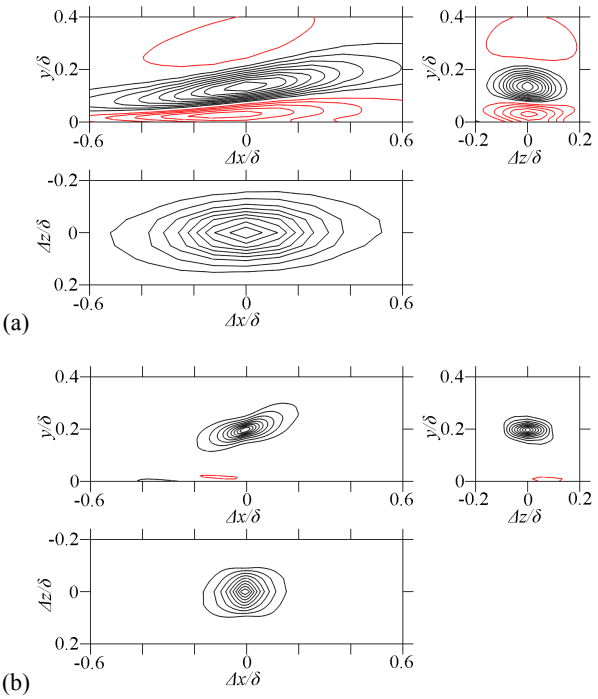

Figure 10. Two-point conditional correlation coefficient of ω'_x. One contour level denotes 0.1. Black and red lines represent positive and negative, respectively. (a) Smooth channel, $y_{ref}/\delta \approx 0.13$; (b) Case F-3, near mid-cavity, $y_{ref}/\delta \approx 0.2$.

An explanation for a smooth channel has been made by Jeong et al. (1997). The negative correlation near the wall is due to opposite-signed ω'_x induced by the no-slip condition. A negative correlation near the rough wall hardly seen, but it can be seen when the reference point is moved toward the wall. The positive correlation lengths are shorter than the smooth channel, especially in the streamwise direction. Whereas an inclination angle in the x-y plane is smaller than 10° in the

smooth channel, the angle is nearly 20° in the rib cavity. These results correspond to the instantaneous field. The increased angle produces rotation on the wall-normal direction.

Figure 11 shows the two-point correlation of ω'_z:

$$R_{\omega_z\omega_z} = \frac{\overline{\omega'_z\left(x_{ref}, y_{ref}, z\right)\omega'_z\left(x, y, z+\Delta z\right)}}{\omega'_{z,rms}\left(x_{ref}, y_{ref}\right)\omega'_{z,rms}\left(x, y\right)}. \qquad (8)$$

The correlation distributions in the smooth channel resemble that of ω'_x. However, the inclination angle in the x-y plane is near zero in the rough channel and a local maximum is shown behind the trailing edge of the rib. Therefore, the correlation of ω'_z in the rough channel seems to show spanwise vortex structure.

Although the turbulent structure near the rough wall leads toward isotropic turbulence, coherent structures exist and produce the high correlation between u' and v'.

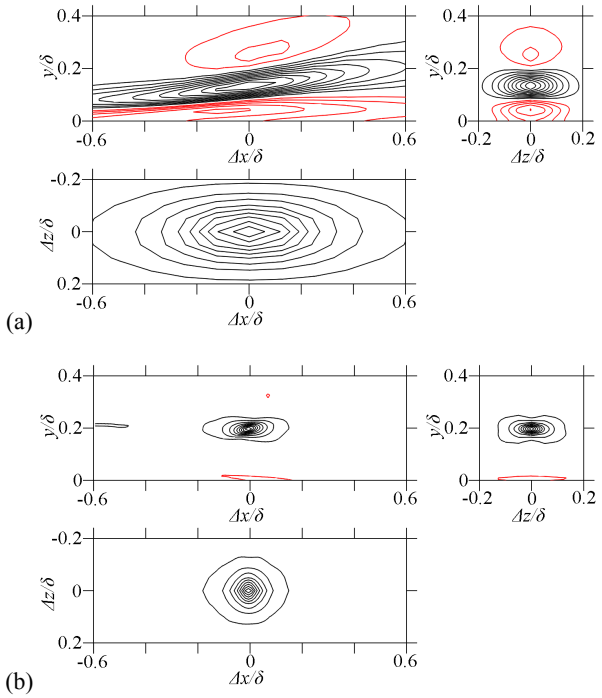

Figure 11. Two-point correlation coefficient of ω'_z. One contour level denotes 0.1. Black and red lines represent positive and negative, respectively. (a) Smooth channel, $y_{ref}/\delta \approx 0.13$; (b) Case F-3, near mid-cavity, $y_{ref}/\delta \approx 0.2$.

CONCLUSIONS

The present paper described the result of DNS for spatially developing turbulent flows in a ribbed channel. The conclusions can be summarized as follows:

- Although the apparent friction factor decreased as flow goes downstream in the case of Pi/H = 2, it increased after unsteadiness in the case of Pi/H = 7 due to the turbulence enhancement.
- For Pi/H = 7, the developing flow near the rough wall even in the second cavity had a similar turbulent structure to the fully developed flow, whereas developed structures spread to the outer.
- Vortex structures were revealed by instantaneous fields and the two-point correlation of vorticities. Streamwise and spanwise vortices appeared in the ribbed channel. This streamwise vortex was smaller than that in the smooth channel, especially in the streamwise direction, and the inclination angle of the vortex was larger.
- The Reynolds normal stress anisotropy near the rough wall was reduced as compared to the smooth wall. However, the Reynolds shear stress showed increased anisotropy corresponding to the intensified correlation between the fluctuations.

REFERENCES

Ashrafian, A. and Andersson, H. I., 2006, "The structure of turbulence in a rod-roughened channel," *Int. J. Heat Fluid Flow*, Vol. 27, pp. 65-79.

Hanjalić, K. and Launder, B. E., 1972, "Fully developed asymmetric flow in a plane channel," *J. Fluid Mech.*, Vol. 51, pp. 301-335.

Ikeda, T. and Durbin, P. A., 2007, "Direct simulations of a rough-wall channel flow," *J. Fluid Mech.*, Vol. 571, pp. 235-263.

Jeong, J., Hussain, F., Schoppa, W. and Kim, J., 1997, "Coherent structures near the wall in a turbulent channel flow," *J. Fluid Mech.*, Vol. 332, pp. 185-214.

Kim, J. and Moin, P., 1985, "Application of a fractional step method to incompressible Navier-Stokes Equations," *J. Computational Physics*, Vol. 59, pp. 308-323.

Leonardi, S., Orlandi, P., Djenidi, L. and Antonia, R. A., 2004, "Structure of turbulent channel flow with square bars on one wall," *Int. J. Heat Fluid Flow*, Vol. 25, pp. 384-392.

Matsubara, K., Kobayashi, M. and Maekawa, H., 1998, "Direct numerical simulation of a turbulent channel flow with a linear spanwise mean temperature gradient," *Int. J. Heat Mass Transfer*, Vol. 41, pp. 3627-3634.

Miura, T., Matsubara, K. and Sakurai, A., 2010a, "Heat transfer characteristics and Reynolds stress budgets in single-rib mounting channel," *J. Thermal Science Technology*, Vol. 5, No. 1, pp. 135-150.

Miura, T., Matsubara, K., Nagai, Y. and Sakurai, A., 2010b, "Turbulent flow and heat transfer in initial stage of ribbed channel," *Proc. 14th Int. Heat Transfer Conference*, Washington DC, USA, IHTC14-22048, 10pp.